Short-term effects of aerosol on the layer near the ground in a cloudless atmosphere

By WILFORD G. ZDUNKOWSKI and NEIL D. MCQUAGE,[1]
University of Utah, Salt Lake City, Utah, USA

(Manuscript received November 22, 1971; revised version February 8, 1972)

ABSTRACT

The short-term effect of dense atmospheric haze upon the temperature regime of the lower atmosphere is predicted. This is accomplished by solving numerically approximate expressions of the equations of radiative transfer, heat conduction, eddy diffusion and wind motion. In the absence of advection, the influence of haze upon the vertical wind distribution is determined also. In order to visualize the effect of haze more clearly, it is assumed that clouds are completely absent during the prediction period. Four model cases are considered which differ only in roughness height and the geostrophic wind speed.

A mid-latitude winter-time situation is studied at which haze problems are particularly severe. The effect of haze is estimated by predicting the behavior of the air layer near the ground for a haze-free and severely turbid environment. The two situations are then compared to evaluate the effects produced by the presence of haze.

Some calculations are carried out using the particular atmospheric model with ground haze concentration of 400 $\mu g/m^3$, roughness height of 1 cm and geostrophic wind of 5 m/sec. For a winter-time prediction period, starting at the time of sundown, it is found that at sunrise of the first day, the surface temperature of the earth is about 2 degrees higher than one would find in the absence of any haze, other conditions remaining the same. If the haze continues to persist, the nocturnal temperature environment is reversed. It is found that the surface temperature is about 2°C and 4°C lower than the respective temperatures in haze-free air at sunrise of the second and third day of the prediction period.

Mid-day temperatures at the earth's surface are substantially lower in the hazy than in the haze-free atmosphere. After a prediction period of three days, a temperature difference of about 19 degrees is observed. Furthermore, the presence of haze has a pronounced effect on the daytime wind spirals.

1. Introduction

Very recently, Atwater (1971 *a*) presented a fairly detailed account of the influence of aerosol and pollutant trace gases upon the development of vertical temperature profiles in heavily polluted areas. He schematized the solar and infrared spectrum of aerosol particles by assuming values of the complex index of refraction. Thus, he was able to obtain aerosol attenuation parameters by applying Deirmendjian's (1969) realistic aerosol particle distribution function.

Atwater (1971 *b*) assumed that radiative processes are predominant in the formation of the vertical temperature profiles and disregarded the modifying influence of any other heat budget components. This made it necessary to prescribe the surface temperatures to act as forcing functions on the infrared cooling rates. Nevertheless, with the aid of his fairly elaborate yet approximate model, he was able to account for certain realistic features of observed temperature inversions. Atwater (1971 *b*) recognized the need to combine the

[1] Present affiliation: United States Air Force, Wright-Patterson Air Force Base, Ohio 45433, USA.

radiative treatment with other heat budget components to obtain a more realistic temperature prediction model.[1]

At the appearance of Atwater's paper, the present investigation was already concluded and perhaps may be considered as an extension of Atwater's work since the present analysis takes into account the effects of heat conduction and vertical mixing in addition to radiative transfer. It is regrettable that the present investigators were not aware of Atwater's (1971) research so that they developed an independent but not quite as detailed radiation model, thus making comparison of results very difficult.

A truly accurate treatment of the present topic is extremely difficult. For example, such a treatment requires the inclusion of the complete radiative transfer equation taking into account all orders of scattering processes of solar as well as of infrared radiation. Radiative computations would then be carried out for numerous spectral intervals and the results summed over the spectrum. Since the haze concentration changes continually in height and time, these radiative computations would have to be carried out numerous times to obtain radiative temperature changes. Such a detailed treatment is not possible even with the most advanced computers.

For this reason, it is imperative to use approximate methods. It is assumed that heating effects of solar radiation in the atmosphere can be disregarded and that the global radiation at the ground is sufficiently well expressed in terms of Linke's turbidity factor. A detailed discussion of the consequence is given in the "Concluding Remarks", and it is pointed out that neglecting heating by solar radiation is thought to be of minor influence only for the present model cases.

Infrared radiative fluxes and their divergence are approximated by disregarding scattering effects of haze particles. Absorption of infrared radiation by haze, however, is included in radiative temperature change computations making use of properly determined Mie absorption cross-sections. In order to avoid spectral computations which require a huge amount of computer time, spectrally averaged absorption coefficients are introduced. Such simplifications are compatible with other approximations mentioned previously.

Exchange processes are carried out primarily on the basis of Blackadar's (1962) description of the exchange coefficient as modified by Wu (1965). The transport equations of heat and particulate matter together with the equation of motion in simplified form are solved to obtain the temperature distribution of the boundary layer. To make the mathematical treatment tractable it is assumed for wind computations that air density and the geostrophic wind are constant in height and time in the boundary layer. Advection effects are disregarded also.

Four different model profiles are investigated which differ only by the roughness of the ground and the magnitude of the geostrophic wind. Model I uses a geostrophic wind of 5 m sec^{-1} and a roughness height of 1 cm. It is studied for a prediction period of 3 days. Model II, having a geostrophic wind of 10 m sec^{-1} and the same roughness height is examined for a period of 1 day. Model III uses a roughness height of 10 cm, a geostrophic wind of 5 m sec^{-1} and is studied for a period of one day. A limiting artificial situation, Model IV, is studied assuming that there is no wind at all. All models are applied to a winter time, mid-latitude situation (sunrise at 7:35 — sunset at 4:25, 45° N) when haze problems are particularly severe. The beginning time of the temperature prediction is sunset in all cases. The initial concentration of haze is exponentially decreased with height from a maximum value of 400 $\mu g\ m^{-3}$ at the ground.

2. Mathematical analysis

2.1. Definition of symbols

In order to avoid lengthy definitions of physical quantities later on, those symbols are simply listed here which do not require special attention. The less common notation is defined at the appropriate place in the text.

[1] When the manuscript was nearly in final form, Mitchell's (1971) interesting article on the "Effect of Aerosol on Climate ..." became available. The present paper represents no attempt to estimate long-range aerosol effects on climate and thus no comparison of his and the present paper will be made.

λ	Wave length of thermal radiation
σ	Stefan-Boltzmann constant
l	Atmospheric mixing length
k	Karman's constant
g	Acceleration of gravity
θ	Potential temperature
T	Air temperature
T_s	Soil temperature
z, t	Height and time coordinates
u, v	Components of the wind velocity along the x and y axis, respectively
f	Coriolis parameter
$\mathbf{V}_g$, $\mathbf{U}$, $\mathbf{K}$	Geostrophic wind vector, wind vector, vertical unit vector
q	Haze concentration
ϱ	Density of the air
c_p	Specific heat of the air
p	Atmospheric pressure
ϑ_0	Solar zenith angle

2.2. *Treatment of solar radiation*

The approximate, yet fairly reliable, treatment of radiative quantities makes use of Linke's turbidity factor which is described briefly to begin with. Consider the extinction of the parallel solar radiation of extraterrestrial intensity $J_{0,\lambda}$ as it penetrates the ideal Rayleigh atmosphere. The solar intensity reaching the ground is then given approximately by

$$J_g = \int_{0.3\mu}^{3.0\mu} J_{0,\lambda} \exp(-\beta_{R,\lambda} m_l)\, d\lambda \tag{1}$$

where $\beta_{R,\lambda}$ is the dimensionless molecular extinction coefficient pertaining to the homogeneous atmosphere while m_l stands for the relative air mass. One formally writes (Foitzik & Hinzpeter, 1958)

$$J_g = J_0 \exp(-\beta_R m_l) \tag{2}$$

and obtains

$$\beta_R = \frac{1}{m_l}\left[\ln J_0 - \ln \int_{0.3\mu}^{3.0\mu} J_{0,\lambda} \exp(-\beta_{R,\lambda} m_l)\, d\lambda\right] \tag{3}$$

Similarly, one finds equivalent coefficients for haze extinction, β_h, and water vapor absorption, β_w. These three quantities determine Linke's turbidity factor

$$\tau_L = (\beta_R + \beta_h + \beta_w)/\beta_R \tag{4}$$

which is approximately independent of the relative air mass as again verified by this study. For practical computations β_R is not found from (3) but from an equivalent empirical relationship proposed by Feussner & Dubois (1930).

$$\beta_R = \ln \frac{1}{0.907\, m_l^{0.018}} \tag{5}$$

The computations of β_h and β_w are based on the haze attenuation and water vapor absorption constants listed by Zdunkowski & Weichel (1971) and Zdunkowski & Strand (1969), respectively. Additional details are given later on.

During the daytime, the earth's surface is illuminated by the global radiation $G(\vartheta_0, \tau_L)$ which is the sum of the diffuse and the direct solar radiation. The global radiation varies with turbidity and also with the position of the sun. The variation of the solar zenith angle as a function of the time of the year and day as well as the latitude is easily established from a well-known relationship of mathematical astronomy and is not reproduced here. For the reasons stated in the introduction, $G(\vartheta_0, \tau_L)$, for a great variety of conditions, cannot be obtained in an exact manner, not even with the most advanced present-day computers. For this reason, certain approximations are adopted which follow essentially the outline of Philipps (1962) whose paper is not readily accessible.

For the computation of the direct solar radiation in a turbid atmosphere, one may use the generalized interpolation formula (5)

$$\begin{aligned} J_g' &= J_0 \left[\frac{0.907}{(\cos\vartheta_0)^{0.018}}\right]^{\tau_L/\cos\vartheta_0} \cos\vartheta_0 \\ &= D(m_l, \tau_L)\, J_0 \cos\vartheta_0 \end{aligned} \tag{6}$$

where m_l is replaced by sec ϑ_0. Combining i_0, which denotes the diffuse radiation of the atmosphere, and J_g' it is possible to define the ratio

$$\Lambda = \frac{i_0}{J_0 \cos\vartheta_0 - J_g'} = \frac{i_0}{J_0 \cos\vartheta_0 (1-D)} \tag{7}$$

which applies to the turbid haze atmosphere. After Bernhardt & Philipps (1958) this quantity is nearly independent of the relative air mass and assumes the approximate value $\Lambda = 0.34$. Assuming a uniform reflectivity of the ground, r', the global radiation, after reflection, is given by

$$G(r', \vartheta_0, \tau_L) = (i_0 + J_g')(1 - r')$$
$$= J_0 \cos\vartheta_0 (1 - r')(\Lambda - \Lambda D + D) \quad (8)$$

Equation (8) requires the knowledge of $D(m_l, \tau_L)$. For various turbidity factors, the same authors find average values of $D(m_l, \tau_L)$ which are formed with the aid of (6) for solar zenith angles ranging from twenty to eighty degrees. It is found that the deviation of $D(m_l, \tau_L)$ from the average value $D(\tau_L)$ is relatively small and that $D(m_l, \tau_L)$ can be approximated by the linear relation

$$D(\tau_L) = 0.82[1 - 0.116(\tau_L - 1)] \quad (9)$$

Combining (8), (9), and assuming an average reflectivity $r' = 0.15$, the global radiation is finally given as

$$G(r', \vartheta_0, \tau_L) = J_0(0.802 - 0.054\,\tau_L)\cos\vartheta_0 \quad (10)$$

This equation is now directly applicable for a given measure of turbidity.

2.3. *Treatment of long wave radiation*

In order to carry out the analysis in an efficient manner, all radiation computations are based on transmission functions which are free from wave-length. Such transmission data, for example, can be obtained from radiation charts of free air measurements. For boundary layer computations, it is permissible to disregard the temperature dependency of the transmission function so that the simple emissivity method becomes applicable. In order to keep the complexity of the overall computational procedure within certain limits, it is thought permissible to disregard the radiative effects of carbon dioxide so that flux computations are based on the contributions of water vapor and haze only. For this two-component non-scattering atmosphere, the radiative transfer equation is approximated as described by Zdunkowski (1963) whose final equations are given next for ease of reference. Let w and h stand for the water vapor and haze optical pathlengths, respectively. In terms of the emissivities, ε_w and ε_h for water vapor and haze, the effective mean temperature, T_E, the downward flux (see Fig. 1) originating from an atmospheric slice and arriving at the reference level is given by

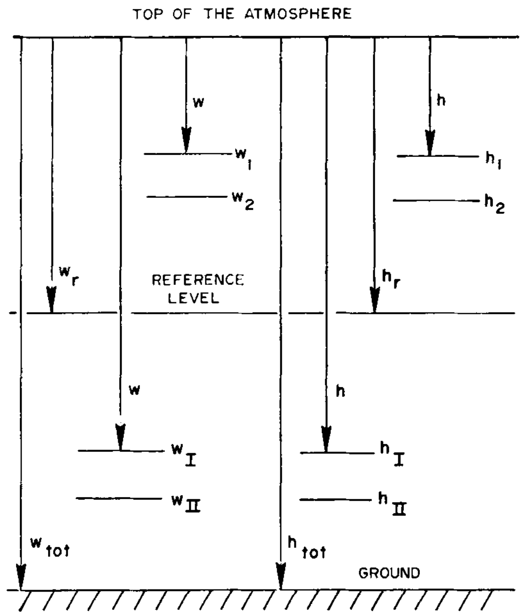

Fig. 1. Optical pathlengths of water vapor and haze as required for evaluation of Eq. (11a, b).

$$\begin{aligned}\Delta F^{\downarrow}(w_r, h_r) = \sigma T_E^4\{&\varepsilon_w(w_r - w_1) - \varepsilon_w(w_r - w_2)\\ &+ \varepsilon_h(h_r - h_1) - \varepsilon_h(h_r - h_2)\\ &\times \varepsilon_w(w_r - w_1)\,\varepsilon_h(h_r - h_1)\\ &+ \varepsilon_w(w_r - w_2)\,\varepsilon_h(h_r - h_2)\}\end{aligned} \quad (11\text{a})$$

The upward flux from a similar layer is found from

$$\begin{aligned}\Delta F^{\uparrow}(w_r, h_r) = \sigma T_E^4\{&\varepsilon_w(w_{II} - w_r) - \varepsilon_w(w_I - w_r)\\ &+ \varepsilon_h(h_{II} - h_r) - \varepsilon_h(h_I - h_r)\\ &- \varepsilon_w(w_{II} - w_r)\,\varepsilon_h(h_{II} - h_r)\\ &+ \varepsilon_w(w_I - w_r)\,\varepsilon_h(h_I - h_r)\}\end{aligned} \quad (11\text{b})$$

The total upward and downward fluxes are then obtained by summation over all contributing atmospheric layers. The upward radiation from the black body ground is accounted for by an additional term.

Whether temperature changes near the ground, the region of main interest, are computed using Möller's (1943) or Kuhn's (1963) data is only of little consequence as follows from Zdunkowski & Johnson (1965). Since Möller's transmission function is known to give reasonably accurate values of the downward flux at the ground, his water vapor emissivity reasonably accurate values of the downward flux at the ground, his water vapor emissivity data are used throughout this study.

The evaluation of the above equations requires the knowledge of the haze emissivities also which are determined upon selection of Deirmendjian's (1964) continental-type haze model. This model is based on actual particle counts and, therefore represents real physical conditions. Lacking a detailed knowledge of actual particle shape, the particle size distribution $n(r)$ is described in terms of equivalent particle radii $r(\mu)$ as

$$\left.\begin{array}{l} n(r) = \text{constant} \times 10^4 \\ n(r) = \text{constant} \times r^{-4} \end{array}\right\} \text{cm}^{-3}\,\Delta\mu \left\{ \begin{array}{l} (0.03\mu \leqslant r \leqslant 0.1\mu) \\ (0.1\mu \leqslant r \leqslant \infty) \end{array}\right. \tag{12}$$

It is assumed in all calculations that the particle distribution function remains unchanged with respect to height and time.

Any exact knowledge of the aerosol index of refraction for the infrared spectrum is missing. Therefore Deirmendjian (1964) and others assume that all haze particles are enveloped by a thin coat of water. Zdunkowski & Weichel (1971) use the index of refraction of water to obtain attenuation coefficients for the entire infrared spectrum. These coefficients are then used to find spectrally averaged haze absorption coefficients, i.e.

$$\bar{\beta}_h = \frac{\int_{3.0\mu}^{92.5\mu} \beta_h(\lambda)\, B_\lambda\, d\lambda}{\int_{3.0\mu}^{92.5\mu} B_\lambda\, d\lambda} \tag{13}$$

which are required for the evaluation of (11a, b). For the range of temperatures considered here, these averaged coefficients are virtually independent of temperature. The haze optical pathlength h is now found from

$$h = \left| \int_{z'}^{z} \bar{\beta}_h\, dz \right| \tag{14}$$

with z' as the reference level height. Finally

$$\varepsilon(h) = 1 - 2Ei_3(h) \tag{15}$$

where Ei_3 represents the exponential integral of the third order.

2.4. The exchange coefficients

The mathematical treatment of the exchange coefficients for momentum K_m and heat flux K_H follow the relationships of Blackadar (1962) for a neutral atmosphere as modified and tested by Wu (1965) to include non-adiabatic conditions.

The resulting relationships are

$$K_m = l^2 \left[\left(\frac{\partial u}{\partial z}\right)^2 + \left(\frac{\partial v}{\partial z}\right)^2 - r_\theta \frac{g}{T}\frac{\partial \theta}{\partial z} \right]^{\frac{1}{2}} \tag{16}$$

$$l = kz/(1 + kz/\lambda_\theta) \tag{17}$$

$$r_\theta = K_H/K_m \tag{18}$$

The parameters r_θ and λ_θ require special treatment. Three discrete zones of stability are recognized in evaluating these parameters: I (unstable), II (between neutral and near-isothermal), and III (inversion). They are approximated as follows:

$$\begin{array}{ll} \text{Zone I:} & \lambda_\theta = U_g \times 10^{-3}/f \text{ and } r_\theta = 1.2 \\ \text{Zone II:} & \lambda_\theta = 2.7 \times 10^{-4} U_g/f \text{ and } r_\theta = 1.0 \\ \text{Zone III:} & \lambda_\theta = 12.5 \times 10^{-5} U_g/f \text{ and } r_\theta = 0.8 \end{array} \tag{19}$$

The value for r_θ is arbitrarily taken as unity by Wu (1965). Here it is permitted to vary slightly to approximate the observed nature of the atmosphere as described by Petterssen (1956).

The behavior of the exchange coefficient at high levels in the atmosphere is not well defined in the literature. It is known that the exchange coefficient decreases from its maximum value in a more or less regular fashion to a residual value at great heights. Such a behavior of the exchange coefficient is not precisely defined from (16) which indeed poses some difficulties in the upper part of the boundary layer. Blackadar, as well as the present investigators, experience the difficulty that the exchange coefficient at great heights does not decrease uniformly, but at times it increases strongly in value. This is not a physically realistic feature which, according to Blackadar, is due to a numerical problem associated with an imperfect satisfaction of the upper boundary conditions. Moreover, Wu's (1965) generalization of the exchange coefficient at times leads to complex values which, of course, is physically unreal.

Below the height where the exchange coefficient reaches its maximum value, no problems are encountered using (16). Here the exchange coefficient is increasing in a regular fashion as expected. In order to obtain a smooth exchange coefficient profile above the height of the maximum value and to avoid the above mentioned problems, it is assumed that K is reduced according to the extrapolation formula

$$K_{m,z} = K_{m,z-\Delta z}\left[\frac{z-\Delta z}{z}\right] \tag{20}$$

whenever required.

This equation is used repetitiously until the fixed, assumed boundary layer height of one kilometer is reached. It is found that at this height the exchange coefficient has a non-zero value which is always greater than or equal to the value of the exchange coefficient at the roughness height. The more advanced approach of the similarity theory can be used also to give a functional form to the exchange coefficient as demonstrated, for example, by Estoque (1963) and Pandolfo et al. (1965). For reasons of simplicity, the second approach is postponed for a later study.

The distribution of the exchange coefficient below the roughness height is not well known and so one depends on estimates. From observational data, Möller (1955) derived that the value of the exchange coefficient at the ground is roughly an order of magnitude larger than its molecular value for nighttime as well as daytime conditions. The distribution of the exchange coefficient in the very lowest layer is then simply approximated by the computed value at the roughness height in conjunction with linear extrapolation to Möller's value. Calculations verify that this technique produces realistic diurnal temperatures near the ground when compared with those discussed by Geiger (1966).

2.5. The prediction equations

It is assumed that the relevant equations governing the fields of heat flow of the boundary and the upper soil layer are given by

$$\frac{\partial\theta}{\partial t} = \frac{\partial}{\partial z}\left(K_H\frac{\partial\theta}{\partial z}\right) - \frac{1}{\varrho c_p}\left(\frac{1\,000}{p}\right)^{0.286}\frac{\partial F_N}{\partial z} \quad z>0, t>0 \tag{20}$$

$$\frac{\partial T_s}{\partial t} = K_s\frac{\partial^2 T_s}{\partial^2_z} \quad z<0, t>0 \tag{21}$$

The boundary statements of this set of equations are given by

$$\left.\begin{array}{ll} T_{\mathrm{AIR}} = T_s & z=0 \\ \theta = \mathrm{const} & z=\infty \\ T_s = \mathrm{const} & z=-\infty \end{array}\right\} \quad t\geq 0$$

$$G(r', \vartheta_0, \tau_L) - F_N + c_p\varrho K_H\frac{\partial\theta}{\partial z} - \varrho_s c_s K_s\frac{\partial T_s}{\partial z} = 0 \text{ for } z=0, \quad t\geq 0 \tag{22}$$

Initial conditions pertain to data representing conditions at the time of sundown.

The vertical distribution of particulate matter of concentration q is given by

$$\frac{\partial q}{\partial t} = \frac{\partial}{\partial z}\left(K_m\frac{\partial q}{\partial z}\right) \tag{23}$$

since it is assumed that the tiny aerosol particles are transported by eddy diffusion in the same way as the air itself. The initial vertical variation of particulate matter is assumed to be given by

$$q(z) = q(0)e^{-0.833\,z}, \quad (z \text{ in km}) \tag{24}$$

which appears to be a reasonable distribution for the lower five kilometers of the atmosphere judging by turbidity measurements as reported by Penndorf (1954). No q-fluxes are permitted at the heights of 0, 1.0 km resulting in the conservation of the total amount of particulate matter. Note that water vapor is not diffused in routine calculations since sample computations indicate that its effect on the total result is very small.

The exchange coefficient distribution requires a knowledge of the wind components. In the absence of advection, these are determined from the horizontal mean wind field as described by

$$\frac{\partial \mathbf{U}}{\partial t} = f(\mathbf{U}-\mathbf{V}_g)\times\mathbf{k} + \frac{\partial}{\partial z}\left(K_m\frac{\partial\mathbf{U}}{\partial z}\right) \tag{25}$$

The component equations are solved subject to the boundary conditions

$$u = v = 0 \quad \text{at } z = z_0$$

$$u = u_g, \quad v = v_g = 0 \quad \text{at } z = \infty$$

In order to evaluate (25), reliable initial data of sufficient resolution must be available for the entire boundary layer. However, such detailed information appears to be absent in the literature. Therefore, it is assumed that initially the atmosphere is in a steady state. Starting values of the wind components are found now according to a method first outlined by Blackadar (1962) for neutral conditions.

An upward marching procedure is used to solve the steady state equivalence of Eq. 25. In such an approach the specification of the lower boundary condition in terms of u, v, u^* and the cross isobar angle ψ_0 is required. The method of selecting the lower boundary condition is outlined below. After initialization, the numerical integration of Eq. 25 is solved as a boundary value problem with u, v specified at both boundaries as previously stated.

In order to initialize the wind distribution, a choice is made of the parameters u^* and ψ_0 for a given value of z_0. These quantities cannot be chosen independently of each other since then the boundary condition at infinity cannot be satisfied in general. An improper choice of u^* and ψ_0 leads to an unreasonable wind distribution. For example, geostrophic wind is computed for unrealistically low heights, or the v-component of the wind does not approach zero.

As an initial approximation for u^* and ψ_0 the predetermined values for the neutral case are chosen. It is known from theory as well as from observation that under stable conditions u^* decreases slightly from its neutral value while the cross isobar angle ψ_0 becomes larger. For given values of u^* and a series of increasing ψ_0-values, trial initial profiles are computed. Finally, u^* and ψ_0 are chosen in such a way that a reasonable Ekman type wind profile is obtained. Additional checks for the choice of the proper u^* and ψ_0 combinations are made on the following basis: 1) The exchange coefficient must approach a small residue value. 2) The maximum value of the exchange coefficient is less than the corresponding value for the neutral case. 3) The height for the maximum exchange coefficient is lower than for the neutral case. It is found that only one particular pair of u^*, ψ_0 satisfies all of the above stated conditions, in addition to giving a reasonable Ekman type wind profile below the geostrophic level.

The height grid used is logarithmically scaled to provide a very dense grid in the vicinity of the earth's surface, the region of strong temperature gradients. There are 51 grid points in height from the 1-meter depth in the soil to the first meter in the air and 44 grid points from here to a height of 1 km. Above 1 km, only radiative temperature changes are important in the present model calculations so that only 9 grid points are needed to the height of the tropopause representing the effective top of the atmosphere. For more details and the numerical evaluation of the prediction equations see Zdunkowski & Trask (1971),

3. Discussion of results

3.1. General remarks

The pressure and initial temperature distribution selected is the "Supplemental Atmosphere, 45 degrees North, January" as given by

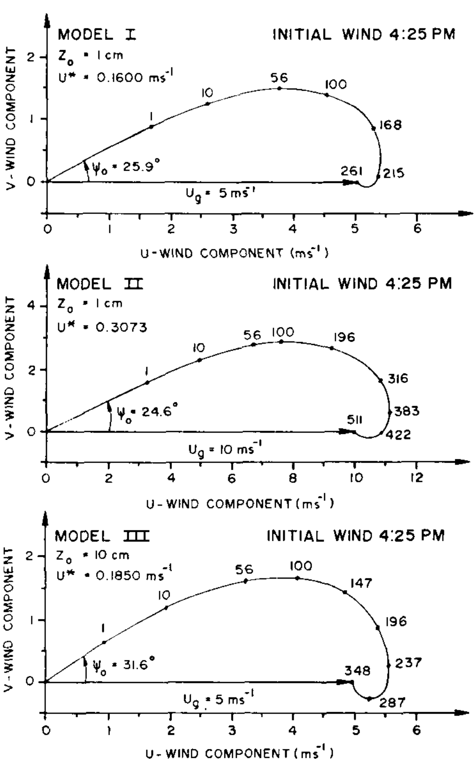

Fig. 2. Initial wind velocity profiles for 3 model cases. Pertinent data are given as part of the diagram.

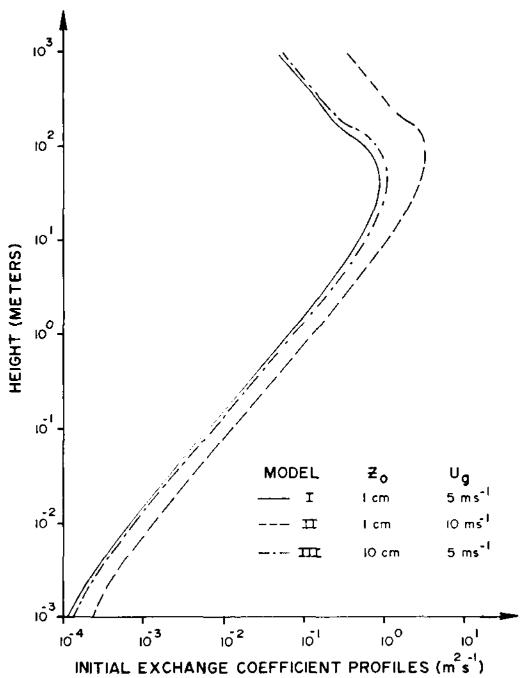

Fig. 3. Initial exchange coefficient profiles for various roughness heights and geostrophic wind velocities corresponding to the 3 model cases.

Valley (1965). Relative humidity is assumed to have a value of 40 % from the ground to a height of 5 km to minimize the potential formation of fog. Above 5 km the relative humidity is decreased to 30 % at the tropopause and then decreased to 0 in the stratosphere.

The soil is assumed to be medium fine, dry quartz sand which is very responsive to temperature changes. Required soil constants are taken from Johnson (1954). The initial distribution of temperature in the soil is taken to be isothermal at 272 K at the surface to a depth of 10 cm and then linearly increased to 282 K at a depth of 100 cm. This is in reasonable agreement with observed winter soil temperature profiles as depicted by Geiger (1966). The soil type and the corresponding temperature distribution largely eliminate the freezing of soil moisture for deeper layers. Possible temperature effects on the soil constants are disregarded.

The selected initial wind and exchange coefficient profiles are depicted in Figs. 2 and 3. Note that some relevant data are stated as part of the figure legend.

Deirmendjian's (1964) continental haze model represents more or less normal conditions resulting in an aerosol mass concentration of only 40 $\mu g/m^3$ and a visual range of roughly 40 km. Such a haze layer causes a nearly negligible additional temperature change for a period of 1 day as compared with haze-free air. In severely polluted air, however, the ground visual range may be as low as 4 km caused by a ground concentration of about 400 $\mu g/m^3$. This larger value is normally used for model concentrations to obtain estimates of possible temperature changes. It is of interest to note that the ratio of the global radiations (Eq. 10) of the aerosol-free air to the heavily polluted air (400 $\mu g/cm^3$ of ground concentration, $\tau_L = 10.7$) results in a value of 3.2.

3.2. *The thermal environment*

Consider the temperature distribution for the 3-day period using Model I which represents a roughness height of 1 cm and a geostrophic wind of 5 m/sec. Fig. 4 indicates that on the first day, the haze produces a warmer nocturnal environment than the haze-free atmosphere.

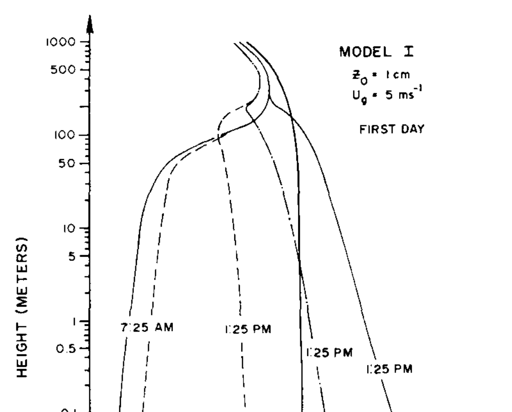

Fig. 4. Selected temperature profiles for Model I, first day of temperature prediction period.

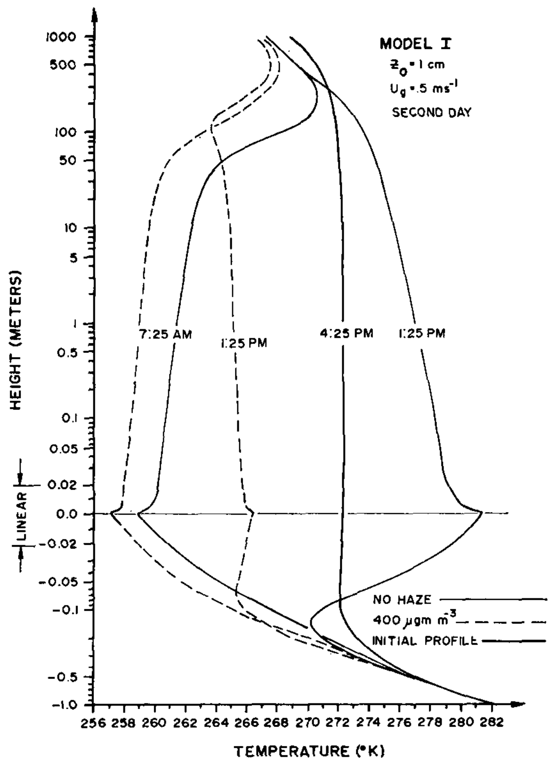

Fig. 5. Selected temperature profiles for Model 1, second day of temperature prediction period.

In contrast, during the daytime, the haze causes a cooler thermal environment than the haze-free air. Note that an afternoon temperature profile for a ground haze concentration of 200 $\mu g/m^3$ is included also. Inspection shows that for this particular model, a linear increase in the haze concentration produces a near-linear reduction in surface temperature.

Fig. 5 depicts for the same model the temperature profiles for the second day of the prediction period. The thermal diurnality of the environment with no haze is generally the same as on the first day. Notice that the reduced solar radiation, due to the presence of haze, during the first day causes a cooler environment to develop during the second night and, of course, during the second day. This indicates that the haze effect of reducing the net loss of long wave radiation at the ground is over-compensated by the reduction of the incoming short-wave radiation. It is noted that potential formation of radiation fog exists just before sunrise.

The temperature profiles for the third day of Model I are depicted in Fig. 6. Here the individuality of the haze environment becomes quite apparent. The haze-free air shows the same thermal cycle previously observed while the presence of haze causes further cooling. At instrument shelter height the mean daily temperature in case of no haze remains at 269 K while the strongly turbid air cools to 265, 262 and 260 K on the first, second and third day, respectively. It is interesting to note that the daily range of temperature in the haze regime remains at about 6 K at shelter height for the 3-day period.

The increased potential for the formation of radiation fog, due to the presence of haze, is now quite apparent. Such fog would form around 5:00 a.m., but its behavior is not predicted.

A comparison of Figs. 4 and 7 shows for the 24-hour prediction period the effect of increased geostrophic wind resulting in increased mixing. Stronger mixing causes an increase in low level temperatures and a reduction in the

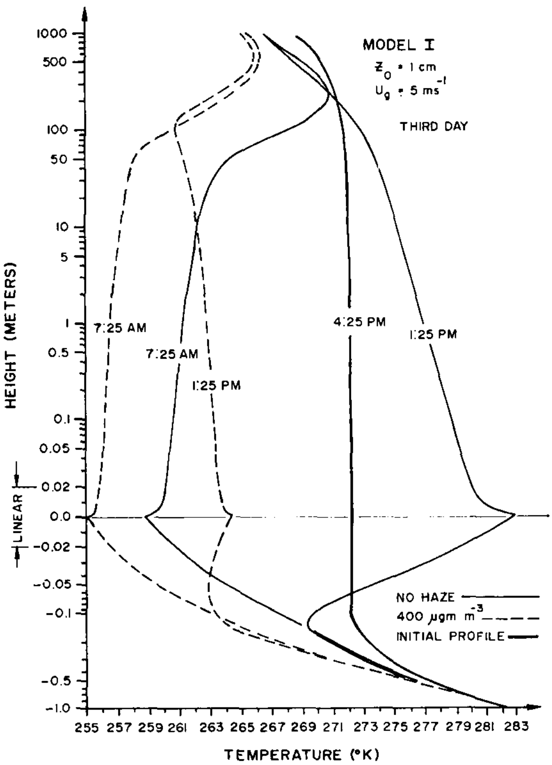

Fig. 6. Selected temperature profiles for Model 1, third and final day of temperature prediction period.

corresponding temperature range. The height of the nocturnal inversion is increased also but the intensity is reduced.

The temperature profiles for Model III, representing the same geostrophic wind as Model I but increased roughness height, are represented in Fig. 8. When compared with Model I (Fig. 4) a slightly decreased temperature range is noticeable. The height of the nocturnal inversion is greater than before but its intensity is reduced. The effect of haze is very similar in both cases.

Fig. 9 considers the physically unrealistic but very interesting hypothetical case (Model IV) that heat transport in the air is carried out only by radiative transport and molecular conduction. Soil heat conduction is the same as in the previous models. The artificial elimination of eddy heat transfer results in a very thin atmospheric boundary layer with the strong temperature gradients shown in Fig. 9. Moreover, the lowest possible ground temperatures are associated with this highly simplified model case, since heat can be transported from the air toward the earth's surface only by the very slow molecular process and by long wave radiation.

The hypothetical model indicates very clearly the role of the exchange processes. In particular, the comparison with Model I (Fig. 4) shows that there exists a strong difference between the midday temperature profiles. In case of non-existing eddy-type heat transport (Model IV, Fig. 9), the atmosphere shows a strong permanent inversion. In comparison, the lapse conditions of the more realistic Model I show the overwhelming role of daytime eddy diffusion in comparison to radiative temperature changes and molecular processes in the air. Heating of the air by solar radiation, neglected in the

Fig. 7. Selected temperature profiles for Model II.
Fig. 8. Selected temperature profiles for Model III.
Fig. 9. Selected temperature profiles for the unrealistic Model IV which disregards eddy exchange processes.

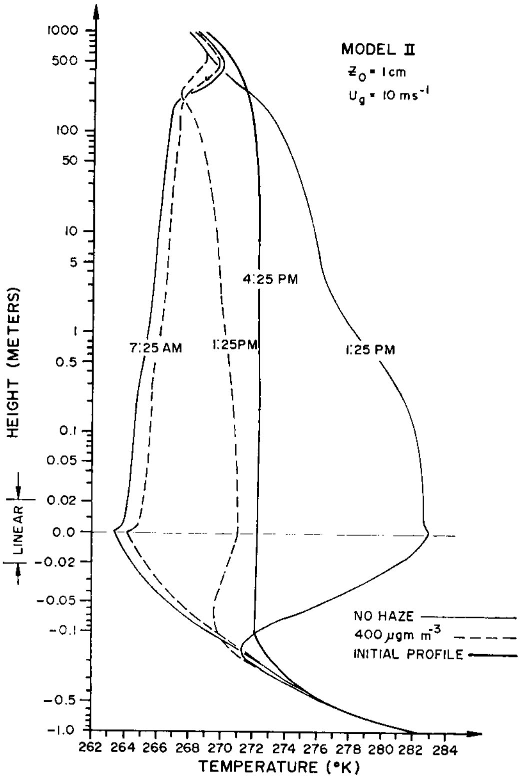
MODEL II
z_0 = 1 cm
U_g = 10 ms^{-1}
7:25 AM
1:25PM
4:25 PM
1:25 PM
NO HAZE
400 μgm m^{-3}
INITIAL PROFILE
HEIGHT (METERS)
LINEAR
TEMPERATURE (°K)
262 264 266 268 270 272 274 276 278 280 282 284

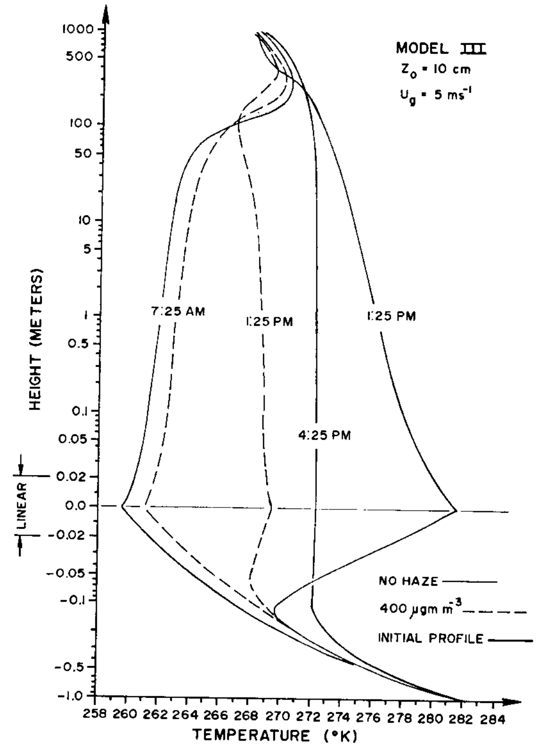
MODEL III
Z_0 = 10 cm
U_g = 5 ms^{-1}
7:25 AM
1:25 PM
1:25 PM
4:25 PM
NO HAZE
400 μgm m^{-3}
INITIAL PROFILE
HEIGHT (METERS)
LINEAR
TEMPERATURE (°K)
258 260 262 264 266 268 270 272 274 276 278 280 282 284

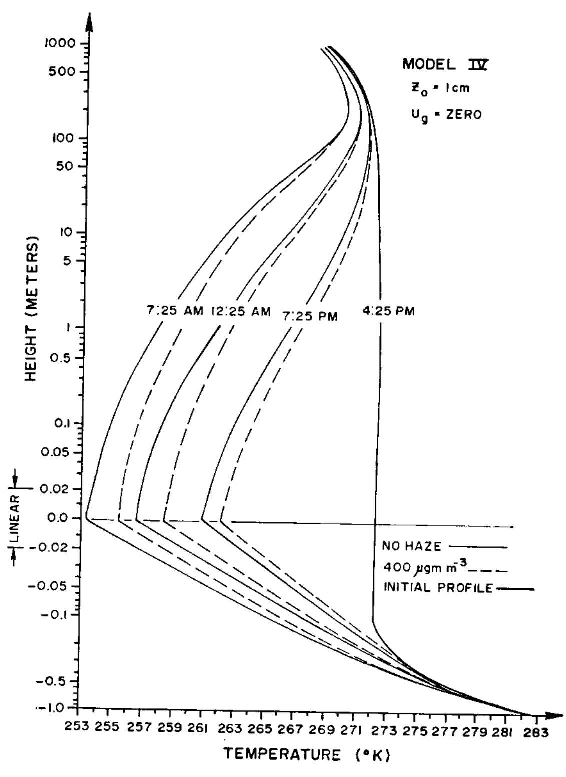
MODEL IV
z_0 = 1 cm
U_g = ZERO
7:25 AM
12:25 AM
7:25 PM
4:25 PM
NO HAZE
400 μgm m^{-3}
INITIAL PROFILE
HEIGHT (METERS)
LINEAR
TEMPERATURE (°K)
253 255 257 259 261 263 265 267 269 271 273 275 277 279 281 283

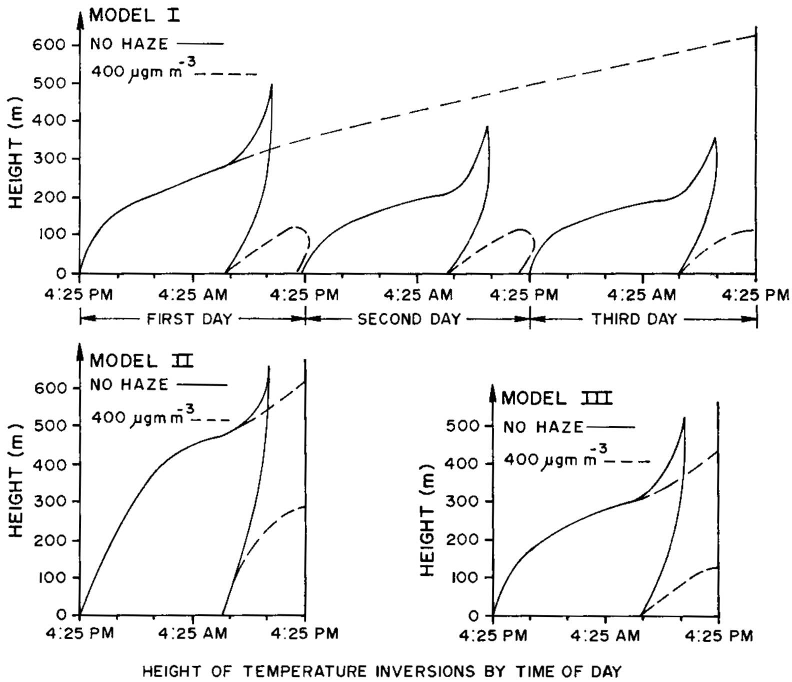

Fig. 10. Height of temperature inversions by time of day for clean and heavily polluted air pertaining to Models I, II and III.

computations, would not change Figs. 4 or 9 substantially as explained in detail later on.

Fig. 10 depicts the growth and cancellation of temperature inversions. Consider the first day of Model I in case of haze-free air. During the night, the height of the inversion increases rapidly at first, then more slowly. After sunrise, the solar heating causes the upper part of the inversion to increase further in height but strongly diminish in intensity. Moreover,

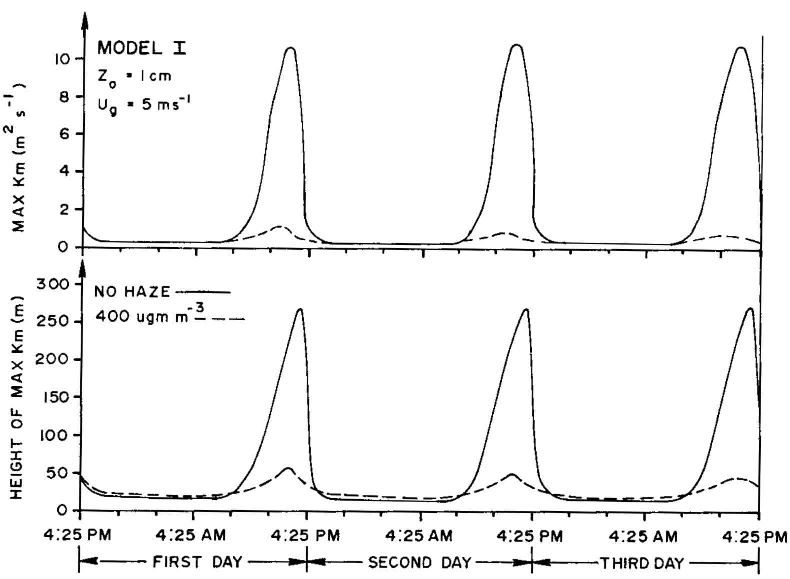

Fig. 11. Magnitude and height of the maximum exchange coefficient vs. time for Model I. Sunset is at 4:25 p.m.

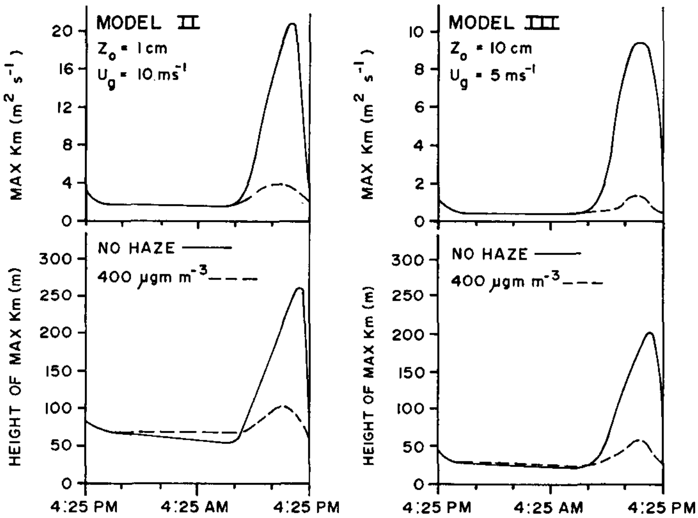

Fig. 12. Magnitude and height of the maximum exchange coefficient vs. time for Models II and III. Sunset is at 4: 25 p. m.

solar heating cancels the ground-based part of the nocturnal inversion which is indicated by the second solid line. By noon, the nocturnal inversion is completely cancelled as shown by the intersection of the two curves. The difference in the height of the nocturnal inversion for the first and second day of Model I indicates that an internal adjustment of the system is taking place. The similarity of the second and third day shows the development of a periodicity in the thermal behavior.

Now consider the aerosol effects in conjunction with Model I. The top of the inversion is rising for the entire 3-day period as indicated by the nearly straight dashed line. At sunrise, the ground-based part of the inversion begins to disappear up to a height of about 100 meters in the early afternoon. Shortly before sundown, inversion conditions are observed everywhere throughout the lower part of the atmosphere. Repetition of these conditions is found for the second and third days. Similar behavior is found for Models II and III. It is seen that in the presence of an intense haze environment, the solar radiation is not sufficient to destroy the entire inversion. This is a model feature which appears to be at least qualitatively in agreement with real atmospheric conditions.

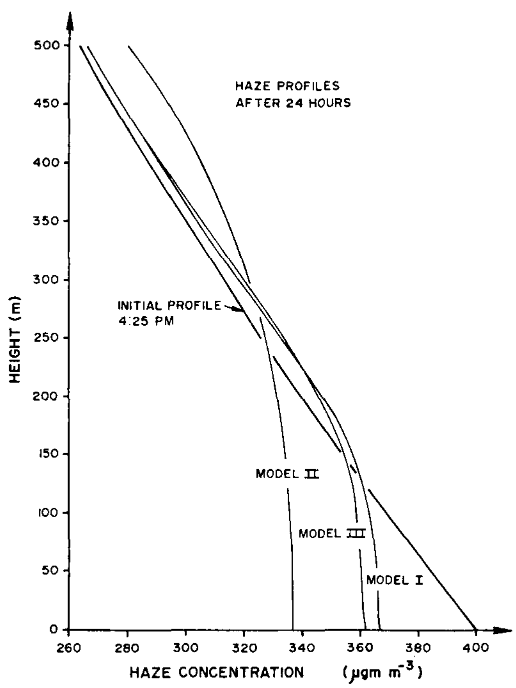

Fig. 13. Haze concentration vs. height after 24 hours of vertical mixing.

3.3. *The exchange coefficient*

The shape of the exchange coefficients profiles are always similar to the initial ones depicted in Fig. 3. There is only a small variation

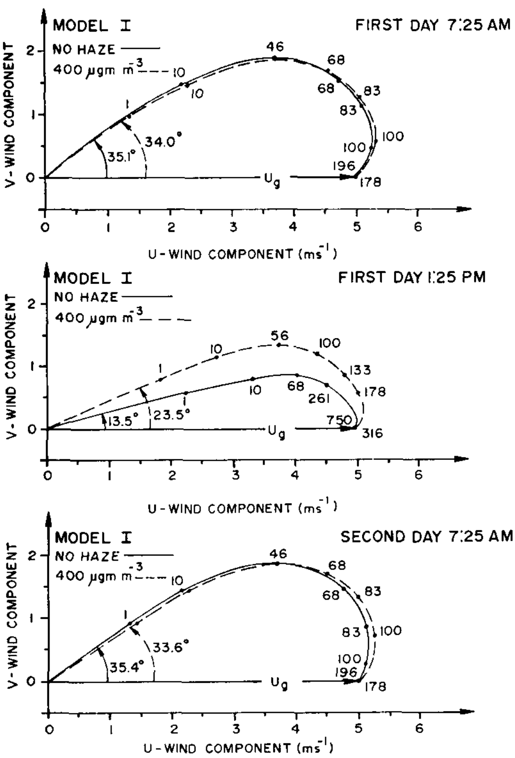

Fig. 14. Selected wind profiles for Model I for the first part of the 3-day prediction period.

near the ground. However, the maximum values of the exchange coefficients and their corresponding heights vary strongly. This is demonstrated in Figs. 11 and 12. Consider first the haze-free air. The exchange coefficient reaches a maximum value in the afternoon. The largest height of the maximum exchange coefficient occurs about an hour later when the entire boundary layer becomes stable.

In the strongly turbid atmosphere during the day, the maximum exchange coefficient increases comparatively little in height or magnitude because of relatively strong thermal stability. In Model II, the greatest value of the maximum exchange coefficient is twice as large as in the other models because of the increased geostrophic wind. The largest value of the maximum exchange coefficient in Model III is the smallest in magnitude when compared to the other models. Notice that the corresponding height is lower also.

3.4. Haze diffusion

Fig. 13 depicts the initial profile of haze concentration and the profiles after a 24-hour period. As expected, the greatest mixing of particulate matter takes place for Model II with the greatest geostrophic wind. The rate of haze diffusion is greatest during the first hour which is caused by the internal adjustment of the system. The total amount of particulate matter in a vertical air column is always conserved as required by the modeling. Examination of Fig. 13 clearly indicates that the amount of haze leaving the lower levels is equal to the amount of haze received in the upper levels.

3.5. The winds

The effect of haze on the vertical variation of the wind of Model I is shown in Figs. 14 and 15. The overall diurnal haze effect slightly increases wind velocities at night but reduces them strongly during the day. This is best

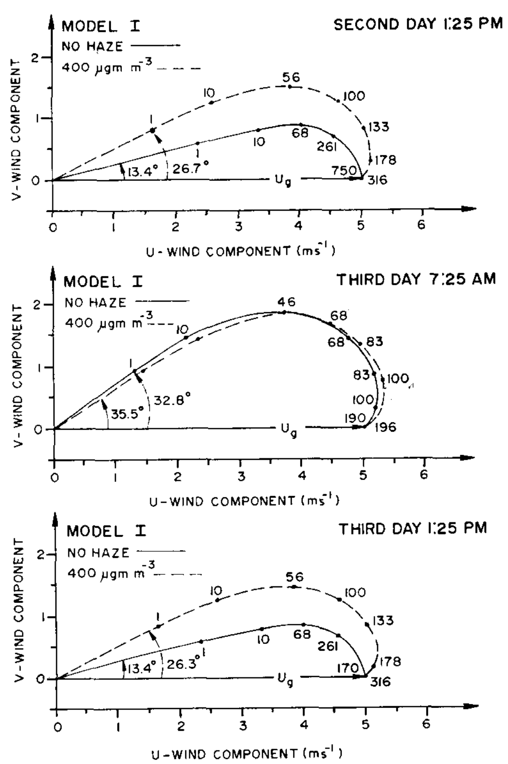

Fig. 15. Selected wind profiles for Model I for the second part of the 3-day prediction period.

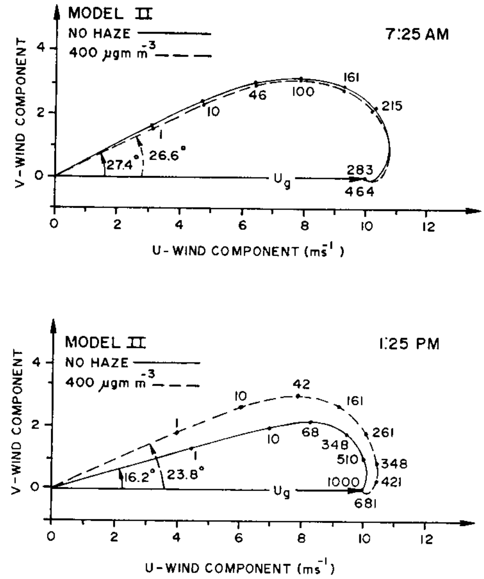

Fig. 16. Selected wind profiles for Model II pertaining to times of sunrise and midday.

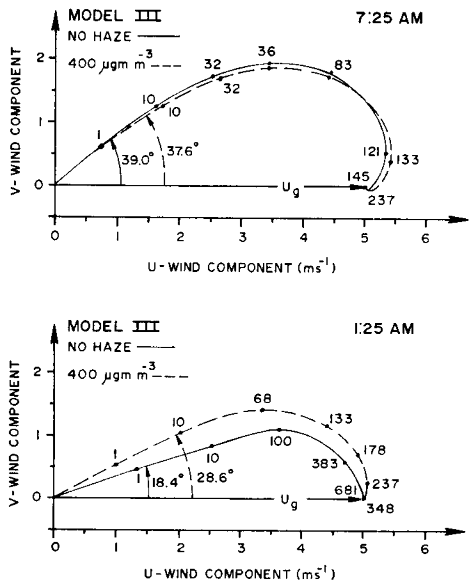

Fig. 17. Selected wind profiles for Model III pertaining to times of sunrise and midday.

observed by comparing the haze-free and polluted atmospheres for 1:25 p.m. on the third day of the prediction period.

In Fig. 16, the effect of haze on Model II is noticeably similar to Model I, but it extends to much greater heights. The nocturnal cross-isobar angle at the ground is considerably smaller than those of Model I. During the day, this effect is reversed and less pronouned.

The morning and afternoon wind profiles for

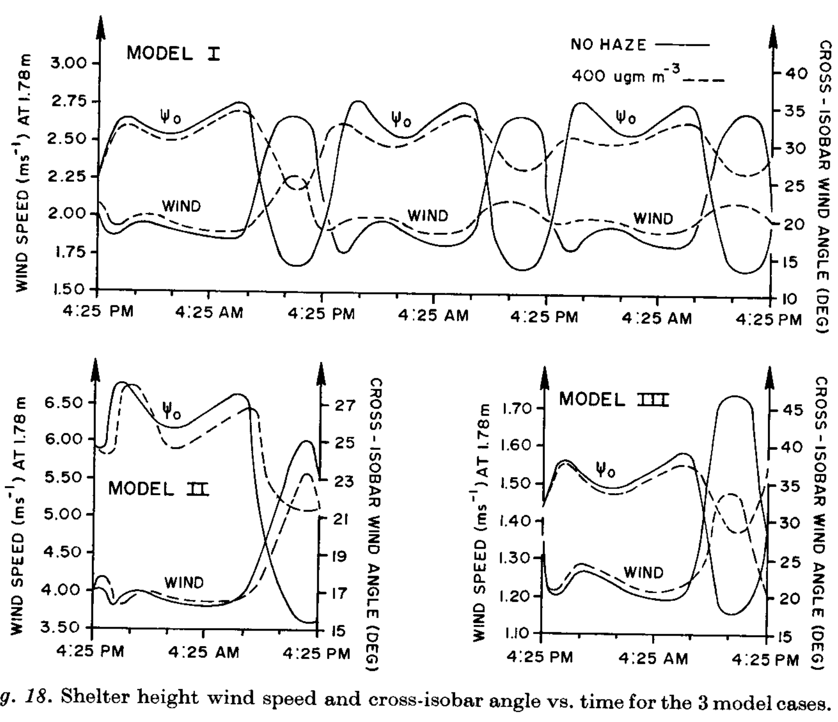

Fig. 18. Shelter height wind speed and cross-isobar angle vs. time for the 3 model cases.

Model III are shown in Fig. 17. The cross-isobar angles produced by a greater surface roughness are larger than those of the other models. The effect of haze on the winds during night and day is quite similar to the other models.

In Fig. 18, the diurnal variation of the wind vector at shelter heights is presented for hazy and haze-free atmosphere for each model. At about 6:00 p.m. one observes a lull in the wind. This coincides with the time of strong low-level thermal stability. At about 9:00 p.m. the wind speed reaches a weak maximum as it readjusts to the decreasing thermal stability. The daily amplitude of this feature decreases in the presence of haze as expected. The most noticeable effect of haze on the low-level wind is during the day.

The variation of the surface cross-isobar angle ψ_0 with time is included also. It has largest and smallest values whenever the wind is smallest or largest, respectively.

4. Concluding remarks

The investigation indicates that the presence of strong haze concentrations in the boundary layer causes a non-negligible reduction of the net infrared radiation loss at the ground. This effect, together with the other heat transfer processes, results in higher temperatures and slightly stronger winds at night than would otherwise be observed in the air layer near the ground for a prediction period of 24 hours.

If haze persists for a period of more than 1 day, the opposite nocturnal effects take place. Persistent haze prevents the ground, and the air layer in contact with it, from warming up during the day to the temperatures observed in haze-free air, other conditions being equal. The diurnal variation of temperature near the ground is found to be substantially less in haze than in "clean" air. The strong effect of haze on the midday wind is demonstrated. Furthermore, the calculations show that haze increases the potential for ground fog formation.

The model considerations are still incomplete in a number of ways. Some shortcomings need to be mentioned. At the time that the present research was carried out, the authors were not aware of existing measured values of the aerosol complex index of refraction for the solar spectrum. Therefore, for the reasons stated previously, the index of refraction of water is used resulting in non-absorbing aerosol for the short wave spectrum.

Atwater (1971), also lacking a detailed description of the index of refraction, more or less arbitrarily specifies the absorption part of the index of refraction as 0.1i for the total solar spectrum. This results in substantial absorption of the solar radiation which is very probably strongly overestimated. According to McClatchey et al. (1970), in their comprehensive report "Optical Properties of the Atmosphere", the aerosol index of refraction is very nearly real (zero imaginary part) for wavelengths less than 0.6 microns. The imaginary value is then more or less linearly increasing to a value of 0.1i at 2 microns. Therefore, approximately 37 % of the solar energy is not susceptible to absorption by aerosol. From the same report, on the basis of the particle distribution function used in this study also, one obtains as a rough estimate an energy weighted average value of the aerosol absorption coefficient of 0.08/km for the rest of the solar spectrum for a haze atmosphere with about 5 km of ground visibility. This visibility value corresponds roughly to the one used in the present study.

One word of caution, it should not be implied that the index of refraction as given by McClatchey et al. (1970) is final. Nevertheless, their result is in rough agreement with Fischer's (1970) absorption measurements on environmental aerosols. He finds an average value of 0.02 for the imaginary part of the index of refraction for the wavelength range from 0.4–1.0 micron.

Atwater (1971) supplies graphs of estimated solar heating for given values of absorption coefficients for the top of aerosol layers where heating is particularly intense. For the absorption coefficient of 0.08/km, for small values of the solar zenith angle, be obtains about 7 degrees of heating per day. To obtain the heating for the solar day, in rough approximation, multiply this number by 0.38 (9 h of sunshine) and by 0.63 (interacting part of the solar spectrum) to obtain aerosol heating rate of approximately 1 and 3/4 degrees.

Now consider radiative heating due to the presence of water vapor. According to Bruinenberg (1946) the solar heating of water vapor, integrated over the solar day, amounts to approximately 0.5 to 1 degree per day for a mid-latitude situation. The combined radiative heating per solar day, disregarding any overlapping action, is then about 2.5 degrees. In the lower few meters of the atmosphere, according to Zdunkowski & Stowe (1967), the infrared cooling of carbon dioxide is of the same order of magnitude. By disregarding both infrared cooling of carbon dioxide and solar heating, one obtains at least a partial cancelling of the errors. Finally, temperature changes of the air and the underlying ground due to daytime exchange processes outweigh by far the effect of atmospheric and solar radiation of the estimated magnitude so that the omission of solar heating and CO_2 infrared cooling should not cause any large errors.

Another shortcoming of this investigation is the omission of horizontal advection. This effect will be included in a future study together with a more sophisticated treatment of the exchange coefficient and the equation of radiative transfer.

Acknowledgment

Gratitude is expressed to the University of Utah for providing free computer time. The authors also appreciate Dr Atwater's comments.

REFERENCES

Atwater, M. A. 1971*a*. Radiative effects of pollutants in the atmospheric boundary layer. *J. Atmos. Sci. 28*, 1367–1373.

Atwater, M. A. 1971*b*. The radiation budget for polluted layers of the urban environment. *J. Appl. Meteor. 10*, 205–214.

Bernhardt, F. & Philipps, H. 1958. Die räumliche und zeitliche Verteilung der Einstrahlung, der Ausstrahlung und der Strahlungsbilanz in Meeresniveau. Teil I, Die Einstrahlung. *Abh. Met. Hydr. Dienstes, DDR, Nr. 45.* Akademie-Verlag, Berlin.

Blackadar, Alfred K. 1962. The vertical distribution of wind and turbulent exchange in a neutral atmosphere. *J. Geophys. Res. 67*, 3095–3102.

Bruinenberg, A. 1946. A numerical method for the calculation of temperature changes by radiation in the free atmosphere (in Dutch). *Kon. Nederl. Meteor. Inst., Meded. en Verhand.* Serie B, Deel 1, No. 1, 57 pp.

Deirmendjian, D. 1964. Scattering and polarization properties of water clouds and hazes in the visible and infrared. *Appl. Opt. 3*, 187–196.

Deirmendjian, D. 1969. *Electromagnetic scattering on spherical polydispersions*, chapt. 3. American Elsevier Publishing Co., Inc., New York.

Estoque, M. A. 1963. A numerical model of the atmospheric boundary layer. *J. Geophys. Res. 68*, 1103–1113.

Feussner, K. & Dubois, P. 1930. Trübungsfaktor, precipitable water, Staub. (*Gerlands*) *Beitr. Geophys. 27*, 132–175.

Fischer, K. 1970. Measurements of absorption of visible radiation by aerosol particles. *Beitr. Phys. Atmos. 43*, 244–254.

Foitzik, L. & Hinzpeter, H. 1958. *Sonnenstrahlung und Lufttrübung*, (chapt. 8.) Akademische Verlagsgesellschaft, Leipzig.

Geiger, R. 1966. *The climate near the ground*, chapt. 2. Harvard University Press, Cambridge, Mass.

Johnson, John C. 1954. *Physical meteorology*, pp. 153–56. M.I.T. Press, Cambridge, Mass.

Kuhn, P. M. 1963. Radiometersonde observations of infrared flux emissivity of water vapor. *J. Appl. Meteor. 2*, 368–378.

List, R. J. 1966. *Smithsonian meteorological tables*, pp. 497–502. Smithsonian Institution Press, Washington, D.C.

McClatchey, R. A., Fenn, R. W., Selby, J. E. A., Garing, J. S. & Volz, F. E. 1970. Optical properties of the atmosphere. AFCRL-70-0527, Air Force Cambridge Research Laboratories, L. G. Hanscom Field, Bedford, Mass.

Mitchell, J. M., Jr. 1971. The effect of atmospheric aerosols on climate with special reference to temperature near the earth's surface. *J. Appl. Meteor. 10*, 703–714.

Möller, F. 1943. Das Strahlungsdiagramm. *Wiss. Abh. Reichsamt Wetterd.*, 9 pp.

Möller, F. 1955. Strahlungsvorgänge in Bodennähe. *Z. Meteorol. 9*, 47–53.

Pandolfo, J. P., Cooley, D. S. & Atwater, M. A. 1965. Further investigations of numerical models of the planetary boundary layer. The Travelers Research Center, Inc., Hartford, Conn.

Penndorf, R. 1954. The vertical distribution of Mie particles in the troposphere. AFCRC Tech. Report 54-5, Geophys. Res. Paper No. 25, Air Force Cambridge Research Center, Air Research Center, Cambridge, Mass.

Petterssen, S. 1956. *Weather analysis and forecasting, vol. II*, chap. 20. McGraw-Hill Book Co., New York.

Philipps, H. 1962. Zur Theorie des Tagesganges der Temperatur in der bodennahen Atmosphäre und in ihrer Unterlage. *Z. Meteorol. 16*, 5.

Valley, Shea L., (ed) 1965. *Handbook of geophysics and space environments*, chapt. 2. McGraw-Hill Book Co., New York.

Wu, S. S. 1965. A study of heat transfer coefficients in the lowest 400 meters of the atmosphere. *J. Geophys. Res. 70*, 1801–1808.

Zdunkowski, W. G. 1963. Untersuchungen über die langwellige Strahlung der Atmosphäre. (*Gerlands*) *Beitr. Geophys. 72*, 103–126.

Zdunkowski, W. G. & Johnson, F. G. 1965. Infrared flux divergence calculations with newly constructed radiation tables. *J. Appl. Meteor. 4*, 371–377.

Zdunkowski, W. G. & Stowe, Jr. L. L. 1968. On

the influence of CO_2 on the radiative flux divergence. *Tellus 20*, 293–299.
Zdunkowski, W. G. & Strand, R. F. 1969. Light scattering constants for a water cloud. *Pure Appl. Geophys. 74*, 110–133.
Zdunkowski, W. G. & Weichel, R. L. 1971. Radiative energy transfer in haze atmospheres. *Beitr. Phys. frei Atmos. 44*, 53–68.
Zdunkowski, W. G. & Trask, D. C. 1971. Application of a radiative-conductive model to the simulation of nocturnal temperature changes over different soil types. *J. Appl. Meteor.* (in press).

КРАТКОСРОЧНЫЕ ЭФФЕКТЫ АЭРОЗОЛЯ НА СЛОЙ ВОЗДУХА ВБЛИЗИ ПОВЕРХНОСТИ ЗЕМЛИ

Предсказывается краткосрочный эффект плотной атмосферной дымки на температурный режим в нижней атмосфере. Это делается путем численного решения приближенных выражений для уравнений переноса радиации, теплопроводности, турбулентной диффузии и движения ветра. Определено также влияние дымки на вертикальное распределение ветра в отсутствие ее адвекции. Для более полного уяснения эффекта дымки предположено, что полностью отсутствуют облака в течение срока прогноза. Рассмотрено четыре модельных случая, различающихся только высотой шероховатости и скоростью геострофического ветра. Изучается ситуация для средних широт зимой, когда влияние дымки особенно сильно. Эффект дымки оценивается путем предсказания поведения слоя воздуха вблизи поверхности земли для случаев отсутствия дымки и сильно замутненного воздуха. Оба случая затем сравниваются. Некоторые расчеты проведены при использовании специальной модели атмосферы с концентрацией дымки в 400 *мкг*/*м*³, высотой шероховатости 1 *см* и геострофическим ветром 5 *м*/сек. Для периода прогноза зимой, начинающегося при заходе солнца, найдено, что к восходу солнца следующего дня температура поверхности земли при прочих равных условиях примерно на 2°C выше, чем в отсутствие дымки. Если дымка продолжает оставаться и далее, то ночные температуры меняются обратным образом. Найдено, что температура поверхности на 2 и 4°C ниже соответствующих температур при чистом воздухе при восходе солнца на второй и третий дни прогноза. Полуденные температуры на поверхности существенно ниже в атмосфере с дымкой, чем в ее отсутствие. После периода прогноза в три дня наблюдается отличие температур около 19°. Присутствие дымки оказывает заметное влияние на поворот ветра с высотой.